

Article

Reexamining Different Factors of the Resonance-Enhanced High-Order Harmonic Generation in Atomic and Nanoparticle Laser-Induced Tin Plasmas

Rashid A. Ganeev^{1,2,3,4,*}  and Hiroto Kuroda^{1,5,6}

- ¹ Ophthalmology and Advanced Laser Medical Center, Saitama Medical University, Saitama 350-0495, Japan; kuroda-alt@theia.ocn.ne.jp
- ² Moscow Institute of Physics and Technology, 141701 Dolgoprudny, Russia
- ³ Institute of Astronomy, University of Latvia, LV-1586 Riga, Latvia
- ⁴ Department of Physics, Voronezh State University, 394006 Voronezh, Russia
- ⁵ Advanced Laser Technology Inc., Tama-city, Tokyo 206-0014, Japan
- ⁶ Plasma Investigations Group, Aichi Medical University, Nagakute 480-1195, Japan
- * Correspondence: rashid_ganeev@mail.ru

Abstract: We reexamine the resonance enhancement of a single harmonic emission during the propagation of ultrafast pulses through atomic and nanoparticle tin-containing laser-induced plasma (LIP). We compare the single atomic Sn and Sn nanoparticle plasmas to demonstrate a distinction in the enhancement factor of the single harmonic in the case of fixed and tunable near-infrared pulses. The analysis of the dynamics of Sn LIP shows the range of optimal delays between heating and driving pulses (130–180 ns), at which the maximal harmonic yield can be achieved. The enhancements of the 17th and 18th harmonics of 806 nm pulses were analyzed in the case of single-color and two-color pumps of LIP, showing up to a 12-fold enhancement of even harmonics in the two-color pump case. We show the enhancement of a single harmonic in the vicinity of the $4d^{10}5s^25p^2P_{3/2} \rightarrow 4d^95s^25p^2$ transitions of Sn II ions and demonstrate how this process depends on the constituency of the plasma components at different conditions of target ablation. The application of tunable (1280–1440 nm) radiation allows for demonstrating the variations of single harmonic enhancement using a two-color pump of Sn-containing LIP.

Keywords: high-order harmonic generation; nanoparticles; tin plasma; resonance enhancement of harmonics



Citation: Ganeev, R.A.; Kuroda, H. Reexamining Different Factors of the Resonance-Enhanced High-Order Harmonic Generation in Atomic and Nanoparticle Laser-Induced Tin Plasmas. *Appl. Sci.* **2021**, *11*, 2193. <https://doi.org/10.3390/app11052193>

Academic Editor: Alessandro Belardini

Received: 6 February 2021

Accepted: 26 February 2021

Published: 3 March 2021

Publisher's Note: MDPI stays neutral with regard to jurisdictional claims in published maps and institutional affiliations.



Copyright: © 2021 by the authors. Licensee MDPI, Basel, Switzerland. This article is an open access article distributed under the terms and conditions of the Creative Commons Attribution (CC BY) license (<https://creativecommons.org/licenses/by/4.0/>).

1. Introduction

Resonance-related effects play an important role in different fields of laser physics and optics. The interest in these effects is related to the possibility of improving various processes during light–matter interactions. One example of the application of the resonance effects in nonlinear optics is the enhancement of high-order harmonic yield during the interaction of strong laser pulses with gases and laser-induced plasmas (LIPs). The studies of this process during the high-order harmonic generation (HHG) of ultrafast laser pulses have been the topic of different publications over the last two decades [1–18]. The HHG model describing the enhancement of the harmonic coinciding with the transition between the ground and the autoionizing states of ions has been developed in [10]. The third (recombination) step of the three-step scenario of HHG was partitioned into two steps: the capture of a laser-accelerated electron onto an autoionizing state of the parent ion, followed by the radiative relaxation of this state to the ground state with the emission of the harmonic photon. Probably, this scenario of resonance HHG could be applied to ionized large particles as well.

HHG in LIPs has actively been studied using different ablated media (bulk metals, organic materials, multiparticle-contained powders, etc. [19–41]). It was mentioned

in previous studies that the enhancement of the resonance harmonics compared with the neighboring ones—in the case, of the nanoparticle-containing plasmas—was notably smaller than in the case of the monomer-containing plasmas [33]. Additionally, different issues require further consideration, once one considers the resonance processes as the suitable method for a single harmonic enhancement. Particularly, tin-containing plasmas, which have earlier been examined as a suitable medium for the demonstration of this effect [42,43], allow for analyzing different processes in various constituents of LIPs. Additionally, the availability of tunable laser sources would allow for determining the influence of the detuning out of resonances on the enhancement factor of a single harmonic.

In this paper, we reexamine the single harmonic resonance enhancement during the propagation of the ultrafast pulses through tin-containing LIP. We demonstrate the enhancement of the 17th and 18th harmonics of 806 nm pulses in the case of different (single-color and two-color) pumps and compare the single atomic Sn and Sn nanoparticle LIPs to demonstrate a distinction in the enhancement factor of a single harmonic in the case of tunable near-infrared (NIR) pulses. The application of tunable (1280–1440 nm) radiation allows for demonstrating the variations of single harmonic enhancement using a two-color pump of Sn-containing plasma.

2. Materials and Methods

Bulk tin (Sn) and Sn nanoparticles (NPs; 70 nm, Sigma-Aldrich, St. Louis, MO, USA), glued onto a glass substrate, were ablated by different laser pulses to form LIP, with further HHG during the propagation of femtosecond laser pulses. The part of uncompressed radiation from a Ti: sapphire laser (central wavelength of 806 nm, pulse duration of 370 ps, pulse energy of 10 mJ, and a pulse repetition rate of 10 Hz) was used as a heating pulse (HP) for the target ablation (Figure 1). We also used a Nd: YAG laser for target ablation, using 1064 nm, 10 ns pulses.

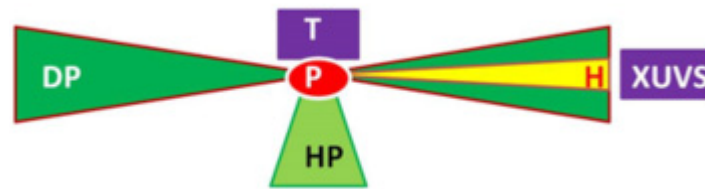


Figure 1. Experimental scheme. DP: driving pulse; HP: heating pulse; T: target; P: laser-induced plasma; H: harmonic emission; XUVS: extreme ultraviolet spectrometer.

The focused compressed (64 fs) driving pulses (DP) were propagated through the LIP at a distance of 0.2 mm above the target surface. Apart from the single-color pump (SCP; 806 nm) of plasmas, we used the two-color pump (TCP; 806 nm and 403 nm) to generate odd and even harmonics. A 0.2 mm-thick beta-barium borate (BBO; type I) crystal was inserted into the vacuum chamber in the path of the focused 806 nm driving pulses to generate a second harmonic ($\lambda = 403$ nm, 3% conversion efficiency).

We also used an optical parametric amplifier (OPA), pumped by the above-described laser, to apply the tunable NIR DP for HHG in the LIP. The signal pulses from the OPA were used as the DP (0.8 mJ, 70 fs, 1280 nm). The intensity of the focused NIR DP inside the LIP was 2×10^{14} W cm⁻². Most of the experiments using the OPA were carried out using the TCP of the LIP. We used the second harmonic (H2) of the signal pulses to apply the TCP scheme (NIR and H2) for HHG in the plasma.

The harmonic radiation was analyzed using an extreme ultraviolet (XUV) spectrometer containing a gold-coated spherical mirror and a 1200 grooves/mm flat-field grating with variable line spacing. The spectrum was recorded on a micro-channel plate (MCP) detector with a phosphor screen, which was imaged onto a charge-coupled device (CCD) camera. The movement of the MCP along the focusing plane of the flat-field grating allowed for the observation of harmonics in different regions of the XUV spectrometer.

3. Results

3.1. 806 nm Pump

The upper panel of Figure 2 shows the raw image of the spectral distribution of plasma emission during ablation of the tin bulk target, using a 370 ps HP at a fluence of $F = 3.2 \text{ J cm}^{-2}$. This spectrum was collected without the propagation of a 64 fs DP through the plasma plume and is shown for the demonstration of various emission lines from highly-ionized tin LIP. The application of such plasma for HHG has two drawbacks: the first disadvantage is associated with strong incoherent radiation in the range of harmonic generation, which can entirely overlap later radiation, and the second disadvantage is related to a deterioration of the optimal phase-matching conditions between driving and harmonic waves. The latter disadvantage leads to a reduction or entire disappearance of harmonic emissions due to a phase mismatch of the interacting waves. In addition, it also affects the conditions for the resonant amplification of harmonics. The propagation of femtosecond pulses through this plasma did not result in harmonic generation or allow for the observation of the weak lower-order harmonics.

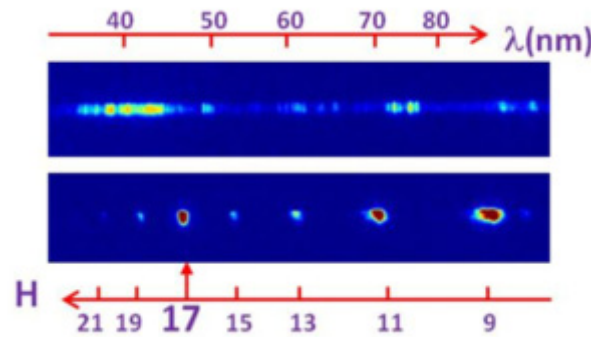


Figure 2. Raw images of plasma (upper panel) and harmonic (bottom panel) emission spectra. Upper and bottom lines show the calibrated wavelength (in nm) and harmonic axes, respectively.

To achieve the efficient generation of harmonics, we used a twice smaller fluence of 370 ps pulses on the target surface (1.6 J cm^{-2}) when no lines attributed to the ionic transitions in this spectral range were observed (bottom panel of Figure 2). The propagation of the DP through such LIP resulted in the generation of an XUV spectrum, comprising the harmonics of 806 nm radiation up to the 21st order (H21). One can see a strong emission attributed to the resonance-enhanced H17 ($\lambda = 47.4 \text{ nm}$), which notably exceeded the nearby harmonics. These studies were performed at a 150 ns delay between the HP and the DP. One can see that the strong H17 almost coincides with the positions of some weak emission lines of the plasma (upper panel of Figure 2). This harmonic was 4 to 10 times stronger than the nearest harmonic orders.

The raw images of the harmonic spectra provide a better comparative view of the plasma and harmonic emissions. The bottom image of Figure 2 shows the common feature of the gradually decaying plateau-like harmonic distribution along the whole studied XUV spectrum except for the single-enhanced harmonic (H17). These raw images were taken at the saturation conditions of the CCD camera for better viewing of the peculiarities of the harmonic distribution. Notice that all line-outs of the harmonic spectra shown in the following figures were taken using the images collected at the unsaturated conditions of registration.

We used two methods to analyze the dynamics of tin plasma spreading out from the target surface. Apart from the plasma emission spectra, we first analyzed the images of the plasma at different moments from the beginning of ablation. Useful information about ablated species can be retrieved by recording the spatial dynamics of the spreading of the plasma plume using a gated intensified charge-coupled device (ICCD) camera, which was used for imaging of the spreading tin LIP within a time interval ranging from 0 to 2000 ns with a variable time gate. In this case, we used 1064 nm, 10 ns pulses as the HP. The used HP energy ($E_{\text{HP}} = 20 \text{ mJ}$) was higher than that used for the harmonic generation, for better

visibility of the plasma plume, while the overall dynamics of the plasma formation and spreading were similar, thus allowing for the determination of the main regularities.

At the initial moments from ablation (i.e., up to 50 ns), the LIP was spatially limited inside the dense and very bright small volume. As it was shown by analysis of the time-resolved spectra of the ns-induced LIP in the visible region [44], a strong continuum emission can be seen at the early periods of plasma dynamics. Neutral emission peaks were not evident at early times in the case of the ns-induced plasma spectra and required longer delays to appear. Additionally, they showed lower intensities compared to the ionic emissions at the early stages. This is attributed to a higher population of the charged ions emitting in the visible region compared to the neutral atoms, though once these ion populations decreased due to recombination processes in the LIP, at later times the emissions from neutral species became a dominating factor. Images in the case of the time delays above 100 ns show a small, expanded laser plume up to a distance of 1.2 mm from the surface of the bulk tin. Due to high brightness, we suppressed emissions by placing neutral filters in front of the ICCD camera. At a period of 200 ns from the ablation, the fastest components of plasma expanded up to a distance up to 2.5 mm. However, their role in harmonic generation is questionable due to a small concentration of these fast components of LIP. We analyzed the images of plasma up to 2000 ns from the beginning of ablation, when a weak, low-dense cloud of plasmas was still seen in the images.

The second method of the plasma dynamics studies was based on the analysis of the variations of harmonic emissions at different delays between the HP and the DP using a two-laser (Ti: sapphire and Nd: YAG) configuration. In this case, HHG spectra from Sn plasma were recorded at different delays between a 10 ns HP and a 64 fs DP. The intensity dependencies of the 11th (H11) and 15th (H15) harmonics on the delay between the HP and the DP are shown in Figure 3A. For this plasma, the maximum delay up to which we were able to observe HHG emission was equal to ~ 500 ns, at which a very weak emission of the lowest recorded harmonic (H9) was still seen in the XUV spectrum. We observed the clearly determined maximal yields of both H11 and H15 at the same (~ 150 ns) delay from the beginning of ablation. This pattern can be explained by the presence of the same type of emitters within the whole period of observation, when a decrease of plasma density, due to its expansion, causes the decay of the harmonic yield. The velocity of these emitters, according to optimal delay, can be estimated at $\sim 1.3 \times 10^3$ m/s, taking into account the 0.2 mm distance between the target and the axis of DP propagation. Notice that a similar range of the “optimal” delays (140–200 ns) between the HP and the DP corresponded to the observation of the maximal harmonic yield in the case of the ablated Sn NP LIP.

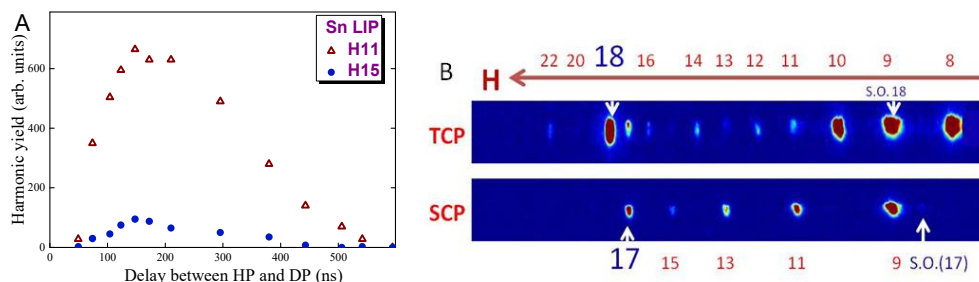


Figure 3. (A) Variations of the 11th (open triangles) and 15th (filled circles) harmonic yields at different delays between the heating and driving pulses. The fluence of heating pulses on the tin surface was 1.5 J cm^{-2} . (B) Raw images of harmonics in the case of a two-color pump (TCP; 806 nm and 403 nm, upper panel) and a single-color pump (SCP; 806 nm, bottom panel) of tin plasma. Arrows show the maximally enhanced harmonics and their second-order (S.O.) diffractions from the flat-field grating in the case of the two types of pumps.

One can note that during the ablation of bulk Sn, the plasma may contain tin atoms and ions, as well as NPs synthesized during laser ablation. The appearance of Sn nanoparticles was commonly registered at the relatively high fluencies of HP ($F \approx 3 \text{ J cm}^{-2}$). The transmission electron microscope (TEM) analysis of the debris deposited on the nearby

glass substrates while using this fluence of either picosecond or nanosecond HP revealed the presence of sparsely distributed NPs with sizes ranging between 2 and 10 nm. Once again, we emphasize that this mode of plasma formation was unsuitable for generating harmonics in Sn LIP. The use of the fluence $F = 1.5 \text{ J cm}^{-2}$, at which the strongest yield of harmonics from this plasma was achieved, did not reveal the presence of NPs in the deposited debris. Thus, the harmonics, in this case, originated from the atoms and ions of tin.

In these experiments, the femtosecond pulses were delayed with respect to those from the Nd: YAG laser to propagate through the formed plasma at a maximal density of the ejected particles. The synchronization of the femtosecond and nanosecond lasers was accomplished using a digital delay generator, and the delay between the HP and the DP was varied in the range of 0 to 1000 ns. We were also able to analyze the plasma and harmonic dynamics at high delays, spanning from a few units to several hundred microseconds. However, apart from the delay region, in which strong harmonics were observed (100–300 ns, Figure 3A), no harmonics appeared in the microsecond-long delays, thus pointing out the absence of the influence of large mass species on the whole yield of harmonic emissions from the tin LIP.

The application of the TCP to this plasma led to the appearance of a rather stronger difference between the whole set of harmonics and one of them, which was attributed to the influence of a resonance-induced mechanism of the enhancement of a single harmonic in the vicinity of the strong transition of tin ions. In the case of the 0.2 mm-thick BBO, some temporal delay between 806 and 403 nm pulses in the LIP still allowed for the effective interaction, leading to the odd and even harmonics generation, since the trailing part of the second harmonic wave overlaps with the leading part of the 806 nm wave (Figure 3B). Another spectrum appeared in the case of the installation of 0.5 mm-thick BBO on the path of the DP. The harmonic distribution became notably heterogeneous due to an insufficient overlap between the 806 nm and 403 nm pulses, delayed from each other by 95 fs in the plasma area, resulting in the generation of $2(2n + 1)$ harmonics (H10, H14, H18, and H22), while other even harmonics, corresponding to $4(n + 1)$ orders (H12, H16, and H20), were almost suppressed.

The most important finding in these TCP studies was the appearance of an exceptionally strong 18th harmonic (upper panel of Figure 3B) notably exceeding the above-analyzed 17th harmonic achieved during the SCP of the Sn LIP. Moreover, second-order diffraction of this harmonic caused a stronger image of H9 (upper right arrow), leading to the impression that H9 became stronger in the case of the TCP compared with the SCP (bottom panel of Figure 3B). The prevalence of H18 over H17 could have been caused by a stronger involvement of the resonance processes in the enhancement of the former harmonic emission. The wavelength of this harmonic (H18, $\lambda = 44.8 \text{ nm}$, $E = 27.68 \text{ eV}$) was closer to some $4d^{10}5s^25p^2P_{3/2} \rightarrow 4d^95s^25p^2$ ionic transitions of tin, possessing strong oscillator strengths (gf). In the meantime, the gf of one of those transitions [$4d^{10}5s^25p^2P_{3/2} \rightarrow 4d^95s^25p^2 (^1D)(^2D_{5/2})$], at the wavelength of 47.20 nm, has been calculated to be 1.52, and this value is five times larger than other transitions from the ground state of Sn II [45]. From this point of view, one can expect an almost perfect coincidence of an H17 ($\lambda = 47.4 \text{ nm}$) and $4d^{10}5s^25p^2P_{3/2} \rightarrow 4d^95s^25p^2 (^1D)(^2D_{5/2})$ transition, and stronger enhancement compared with H18. However, our experiment showed the reverse case when H18 is much stronger than H17.

A few reasons could be responsible for this contradiction. The presence of an even stronger ionic transition of Sn II in the 44 nm range of the XUV spectrum can cause a larger enhancement of H18 with respect to H17. Additionally, the Stark shift of transitions can modify their influence on the harmonic yield. Another option could be the involvement of the Sn III ions [43]. Some of them lie in the vicinity of H18 and their oscillator strengths (gf~0.5) are high enough to cause the resonance enhancement of nearby harmonics. Finally, H18 belongs to the group of $2(2n + 1)$ even harmonics, which can demonstrate larger conversion efficiency compared with the odd harmonics arising from the 806 nm pump.

Notice that the efficiency of harmonics produced by shorter wavelength sources becomes higher due to the strong wavelength-dependent harmonic yield ($I_{\text{harm}} \propto \lambda^{-5}$) (I_{harm} is the harmonic intensity and λ is the driving field wavelength [46]).

3.2. Tunable NIR Pump

One can distinguish the importance of tuning the wavelength of the driving pulses to determine the variations of harmonic yields in the case of resonance-related processes. Therefore, the application of OPA-based tunable sources offers large perspectives in these studies. Below, we apply the tunable NIR pulses from the OPA and their second harmonics for the analysis of resonance enhancement in Sn LIP, as well as in Sn NP LIP.

High-order harmonic generation in two media using TCP pulses was optimized by different means (i.e., the fluence of HP, the intensity of DP, the delay between the HP and the DP, the application of BBO crystals of different thickness, etc.). Particularly, relatively stronger ablation of the Sn NP target allowed for the observation of the enhancement of odd and two neighboring harmonics in the vicinity of a strong ionic transition of tin, contrary to the case of the weak ablation of this nanoparticle-containing target. Our TEM studies of Sn NP debris deposited on nearby glass slides showed the presence of the small NPs ranging from 4 to 14 nm. These NPs appeared in the TEM images at the optimal fluencies of HP ($F = 1.4\text{--}1.7 \text{ J cm}^{-2}$), when the maximal harmonic yield was achieved.

The harmonics in the case of the NIR pulses (1 mJ, 1300 nm) were significantly weaker than in the case of the 3 mJ, 806 nm pump, due to a higher intensity of DP in the latter case, and the $I_{\text{harm}} \propto \lambda^{-5}$ rule. The comparison of these two pumps at similar energies of pulses (1 mJ) showed a four-fold decrease of harmonic yield from the plasma produced on the bulk Sn target in the case of 1320 nm pulses compared with the 806 nm pulses, which, to some extent, corresponds to the theoretical prediction of this ratio (11), taking into account a difference in the spatial distributions of two focused beams in the plasma area. Meanwhile, the harmonic cutoff in the case of the NIR pulses was larger than in the case of 806 nm pulses, in accordance with the expectations in the extension of this parameter for the longer-wavelength pump ($E_{\text{cutoff}} \propto \lambda^2$). The harmonic cutoffs in the case of the 806 nm and NIR pump (~ 1300 nm) pulses were in the range of 42 nm ($E = 29.5$ eV) and 38 nm ($E = 32.6$ eV), respectively, while the expected cutoff was calculated to be 76 eV. However, the very small conversion efficiency of higher-order harmonics in the case of NIR pulses did not allow for the observation of harmonics well below the 40 nm spectral region. Thus, the use of 1-mJ NIR pulses for plasma harmonic studies caused the generation of weak odd harmonics in the longer-wavelength range of the XUV spectrum. For this reason, we used the TCP (NIR and H2) of plasma, which proved to enhance the odd harmonic yield. The extension of the harmonic cutoff compared with the single-color pump, the ten-fold growth of the yield of odd harmonics, the comparable harmonic intensities for the odd and even orders along the whole range of generation in spite of using the 0.5 mm-long crystal, contrary to the case of the 806 nm pump, and the tuning of harmonics that allowed for the optimization of resonance-induced single harmonic generation were among the attractive features of these experiments.

The raw images of the harmonic spectra presented in Figure 4 were obtained using NIR pulses ($\lambda = 1370$ nm) and the second harmonic of this radiation ($\lambda = 685$ nm) during their propagation through the plasma produced on the bulk tin and tin NP targets. As in the case of the 806 nm pump of the Sn LIP, we observed the enhanced harmonic in the region of 47 nm (Figure 4, upper panel). At the used pump conditions, it was the 29th harmonic (H29) of 1370 nm radiation. The application of ablated tin nanoparticles as the media for harmonic generation at the fluence similar to the one used for the ignition of plasma in the case of the tin bulk target ($F = 1.4 \text{ J cm}^{-2}$) allowed for the increase of the conversion efficiency of a whole set of harmonics (Figure 4, middle panel). The harmonics were extended up to the 31st order. However, no variations from the featureless plateau-like pattern of the envelope of the gradually decaying harmonic distribution were achieved in this case, except for some insignificant differences in the intensities of H29 and neighboring orders. This difference in

the harmonic spectra produced from the plasmas ignited on the bulk Sn and Sn NP targets was attributed to an insufficient amount of ionized single-particle species in the latter case.

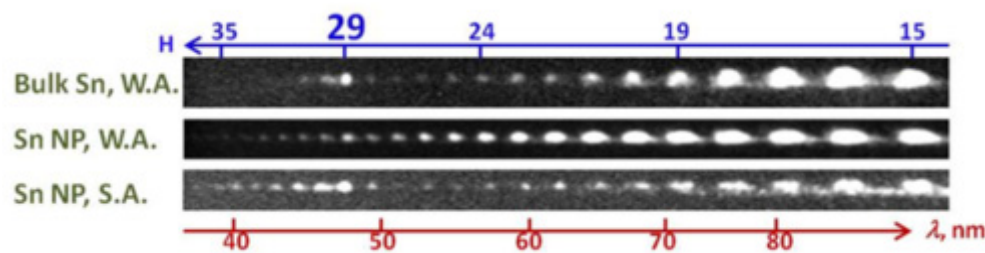


Figure 4. Raw images of harmonic spectra in the case of 1370 nm and 685 nm pumps of tin-containing plasmas. Upper panel: Plasma produced on the tin bulk target at the fluence $F = 1.4 \text{ J cm}^{-2}$. Middle panel: Plasma produced on the Sn nanoparticle (NP) target at the fluence $F = 1.4 \text{ J cm}^{-2}$. Bottom panel: Plasma produced on the Sn NP target at the fluence $F = 2 \text{ J cm}^{-2}$. “W.A.” and “S.A.” correspond to weak and strong ablation of the Sn-containing target.

Changing the ablation conditions of the Sn NP target can lead to the appearance of single-particle species and additional excited states of ions that can, to some extent, amplify the neighboring harmonics. Among different types of ablated substances, tin plasma can be considered as an interesting subject for study since it allows for the modification of the excitation of various autoionizing states, depending on the ablation conditions of the bulk target. The variations of target ablation conditions could allow for the analysis of the nonlinear response of such plasma by comparing the amplification of different harmonics, provided that they coincide or remain close to those autoionizing states responsible for harmonic enhancement. It is interesting to consider this process in the case of the ablation of the targets containing nanoparticles since the modification of their morphology or even the disintegration of NPs into the small species and atoms can drastically change the distribution of harmonics in the region of interest, where strong ionic transitions can cause the enhancement of harmonics in the case of an atomic/ionic plasma medium.

The fluence of heating 370 ps pulses was increased up to $F = 2 \text{ J cm}^{-2}$ to produce a sufficient amount of Sn ions in the plasma ignited on the NP-containing surface. These conditions of ablation proved to be non-optimal for the efficient generation of harmonics. In this case, we observed the worsening of the phase-matching conditions, leading to a decrease in the conversion efficiency of the lower-order harmonics (bottom panel of Figure 4). The appearance of a large number of free electrons at stronger ablation caused the phase mismatch between the harmonic and driving waves, due to the growing group of velocity dispersion in such LIPs. In the meantime, we achieved the enhancement of a single harmonic and a few following harmonic orders in the area of strong ionic transitions of tin. H29, in this case, was notably stronger than any nearby lower-order harmonic, down to H19. Probably, at these conditions of nanoparticle ablation, they disintegrated into smaller nanoparticles, clusters, and single-atomic species, which can be presented in an ionic state, thus allowing the resonance-related enhancement of harmonics.

To further analyze the observed process of the variation of harmonic distribution at different conditions of DP–LIP interactions, we performed the tuning of the driving NIR pulses in the case of two plasmas. The line-outs of Figure 5A demonstrate the harmonic spectra generated in the plasmas produced on the bulk tin and tin NP powder. The three upper panels show the HHG spectra in the plasma produced on the tin bulk target at optimal conditions of ablation when the maximal yield of harmonics was achieved. The upper panel was obtained in the case of the SCP (1355 nm) of the plasma produced on the bulk Sn. One can see the weakly enhanced harmonic (H29) lying far from the whole set of the observed lower-order harmonics. We also used the TCP (1355 nm and 678 nm) of plasma at a similar wavelength of NIR pulses. Again, as in the case of the SCP, H29 and two neighboring harmonics can be clearly distinguished in the 46–48 nm spectral range. The tuning of the NIR pulses towards the shorter wavelength region (1335 nm) caused the change in the maximally enhanced harmonic order in the case of the TCP (H28, 1335 nm

and 668 nm pumps, third panel) and allowed for the generation of a higher yield of this harmonic compared with the neighboring ones.

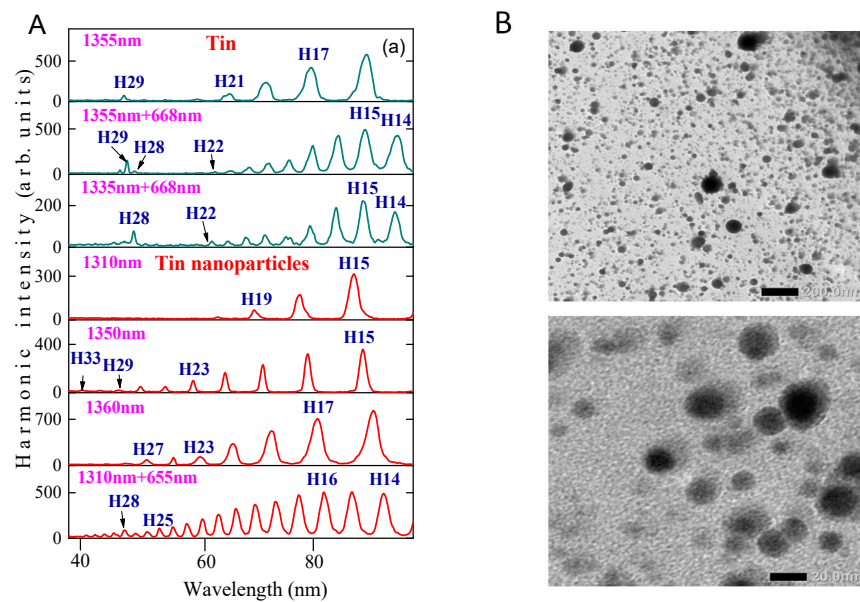


Figure 5. (A) Line-outs of harmonic spectra generated in the plasmas produced on the bulk tin and tin NP powder using tunable near-infrared (NIR) driving pulses. First panel from the top: SCP (1355 nm) of the plasma produced on the bulk Sn. Second panel: TCP (1355 nm and 678 nm) of the plasma produced on the bulk Sn. Third panel: TCP (1335 nm and 668 nm) of the plasma produced on the bulk Sn. Fourth panel: SCP (1320 nm) of the plasma produced on the tin NP powder. Fifth panel: SCP (1350 nm) of the plasma produced on the tin NP powder. Sixth panel: SCP (1370 nm) of the plasma produced on the tin NP powder. Seventh panel: TCP (1320 nm and 660 nm) of the plasma produced on the tin NP powder. (B) TEM images of deposited tin NPs during ablation of nanoparticle powder at an optimal fluence of HP. The black markers correspond to 200 nm (upper panel) and 20 nm (bottom panel).

Similar studies were performed in the case of Sn NP LIP. The application of nanoparticles was a part of our efforts to demonstrate the fact that the presence of tin in plasma does not necessarily guarantee the enhancement of a single harmonic. The decrease of oscillator strength of ionic transitions, as well as the detuning of transitions, can cause the difference in the nonlinear optical response of this medium. Meanwhile, the expectation in the application of NPs was related to the stronger effect of single harmonic enhancement, while our studies showed the reverse effect.

The distribution of the harmonic spectrum was notably changed as soon as we ablated the Sn NP target. One can assume similar conditions for the resonance enhancement of H29 in this aggregated structure. However, in the case of the SCP of Sn NP LIP, we did not observe this process. At the used fluence of heating pulses (1.5 J cm^{-2}), we did not see a strengthening of this harmonic, which points out the insignificant amount of the ionic tin component during the disintegration of Sn NPs in these conditions of ablation, independently of the wavelength of NIR DP.

Specifically, the experimental observations were as follows. The fourth panel from the top of Figure 5A shows the harmonic line-out in the case of the SCP (1320 nm) of the plasma produced on the tin NP powder. Only a few harmonics up to H19 generated at these conditions in the studied spectral range (38–89 nm). The optimization of plasma formation and stronger NIR pulses tuned towards 1350 nm allowed for achieving the harmonics up to H33 (fifth panel). At these conditions, no enhancement of the harmonic lying close to the 47 nm region was achieved. The tunings of the DP (1370 nm) also did not result in the generation of enhanced harmonics in the 47 nm region (sixth panel). Finally, the seventh panel shows HHG using the TCP (1320 nm and 660 nm) of the plasma produced

on the tin NP powder. Again, we did not see the specific feature of single harmonic enhancement in the above-mentioned XUV range, but rather observed the gradual decay of harmonic yield down to H32. An insignificantly larger yield of H28 shown in this panel may indicate the involvement of the resonance process in the generation of this harmonic (similar to the raw image shown in the middle panel of Figure 4 in the case of 1370 nm and 685 nm pumps). The appearance of all even harmonics, in the case of NIR pulses, using thicker (0.5 mm) BBO crystal, revealed a sufficient spatiotemporal overlap of tunable 1300–1370 nm radiation and its second harmonic emission in LIPs due to a lesser difference in the group velocity dispersion of these pulses in the NIR range.

At these conditions of Sn NP ablation, the analysis of debris from the ablated area showed the presence of notably smaller NPs compared with the original 70 nm species glued on the glass substrates. Figure 5B shows two TEM images with different magnification factors of the debris deposited on the nearby substrates, which allow for the determination of the presence of a broad range of the dimensions of nanoparticles (between a few units of nm up to 15 nm). Some smaller clusters yet resolved in these images, being in a plasma state, could be responsible for the resonance enhancement of a single harmonic.

The studies of harmonics using idler pulses (1600–2400 nm) were carried out as well. The harmonics were generated using the wavelengths of a pump close to the regenerative regime of the OPA (1600 nm), due to higher pulse energy. The experiments were carried out in the 1600–1900 nm range. The application of these longer wavelength pumps led to a notable decrease in harmonic generation efficiency due to the $I_{\text{harm}} \propto \lambda^{-5}$ rule. Only the two-color pump configuration was suitable, in this case, to generate odd and even harmonics, while the application of the single-color pump led to a notably weaker harmonic emission. This observation, as well as the above-presented data, points out the attractiveness of the two-color pump over the single-color pump for harmonic generation in laser-induced plasmas, independently on the spectral range of emissions of the fundamental radiation.

4. Discussion

The most important feature of these studies was the availability in the analysis of the excited states influencing the harmonic distribution at different excitation conditions of the ablating target. We presented the results of the harmonic spectra modification using tunable driving two-color (NIR and H2) orthogonally polarized pulses, which led to the observation of the resonance enhancement of some harmonic orders caused by different states of plasmas. Studying resonance-induced enhancement of harmonics using tunable NIR and H2 pulses provides the opportunity to fine-tune this high-order nonlinear optical process for wavelength-dependent enhancement of the harmonic yield. This advantage underlines the attractiveness of the analysis of metals, semiconductors, multi-particle systems, and so forth, and, particularly, of the oscillator strengths of some ionic transitions using the plasma HHG technique. Thus, this approach could be considered as a new method of nonlinear spectroscopy.

The second field (403 nm or 685 nm) breaks the inversion symmetry, which allows for the observation of even harmonics generation forbidden in the case of the 806 nm and 1370 nm pumps. The interaction of a strong fundamental wave (806 nm or 1370 nm) and a weak second harmonic wave (403 nm or 685 nm) in the LIP becomes a sufficient factor to drastically change the spectral pattern of harmonic emissions. Notice that, in this case, the yields of even harmonics were comparable with those of odd ones, in spite of a ~30:1 ratio of the energies of two pumps. The demonstrated effect shows that a weak second field serves as a trigger for the notable change of this nonlinear optical process.

Most of our studies were performed at the fluence $F = 1.6 \text{ J cm}^{-2}$. As we mentioned during the description of the results shown in Figure 4, the growth of the fluence of the 370 ps heating pulses on the target containing Sn NPs allowed for achieving the conditions when the resonance-induced enhancement of the harmonic in the vicinity of strong ionic transitions of Sn becomes pronounced. The disintegration of large NPs into

smaller ingredients (atoms/ions, clusters, and tiny NPs) at these conditions of ablation resulted in the involvement of those ionized species in the process of HHG, followed by the observation of the enhancement of some specific harmonic (either H28 or H29) of the used tunable NIR radiation. The significant suppression of the “resonant”-induced harmonic gain (either the 17th order of the 806 nm pump or 28th and 29th orders of the NIR pump) could have been caused by the shift of the above-discussed transition. However, our experiments using tunable NIR pulses at the fluence of the HP at $F = 1.6 \text{ J cm}^{-2}$ did not reveal the resonance-related processes lead to the enhancement of the harmonic yield. This observation suggests that the tuning of the ionic transition should not be the main factor in leading to the cancellation of the resonance-related effect.

Another factor may be a decrease in the oscillator strength of this transition. The transitions of Sn II and Sn III can be either detuned or weakened once the original species become presented in the form of nanoparticles. The reduction mechanisms of harmonic amplification can be related to either the reduction of the oscillator strength of this transition or the detuning from the wavelength of “resonant” harmonics, or both.

The macroscopic dispersion properties of the plasma could be another key factor for the formation of the resonance-induced enhancement of a single harmonic in tin plasma, as was suggested in [43]. Recent studies of two-component plasmas allowed for analyzing this opportunity in the case of one of the components (Sn) allowing for the generation of enhanced harmonics and the other component (Pb) causing the modification of plasma dispersion properties [47]. The observation of the enhancement of the even (H18) harmonic and the odd (H17) harmonic, in the case of the TCP and SCP of two-component plasma, have demonstrated that the macroscopic properties of the plasma cannot be considered as the origin of the single harmonic enhancement. In other words, the co-existence of lead plasma does not destroy the resonance effect and single harmonic enhancement caused by tin, which suggests the diminished role of the macroscopic effect in the modification of the resonance-enhanced properties of harmonics in the latter component of plasma.

We did not analyze the size-dependent effect of the harmonic yield in the case of nanoparticle-containing plasmas. Meanwhile, the assumption of the influence of a strong local field in the case of smaller-sized nanoparticles, like quantum dots, can predict the growth of harmonic yields in the latter case compared with the large nanoparticles. This assumption can be supported by the vision of HHG as a three-step process, when only atoms on the surface of nanoparticles efficiently participate in harmonic generation, while inner atoms cannot be considered as the emitters of harmonics due to their strong absorbance of generated radiation. The most probable scenario in determining the optimal sizes of atomic aggregates for HHG is the demonstration of the attractiveness of the species with sizes of 1–5 nm, when the quantum confinement effect allows for the increase of the local field-related nonlinearity while limiting the negative effects attributed to the large (20–100 nm) nanoparticles. This assumption has recently been confirmed during the application of metal sulfide quantum dots for HHG [48,49].

There are a few studies of HHG in the plasmas produced on the nanoparticle-coated targets. The aim of those studies was to elevate the nanoparticle cloud by laser ablation (like in our experiments) and to analyze the nonlinear conversion of infrared pulses towards the extreme ultraviolet range. Meanwhile, the most intriguing method would be the propagation of strong laser pulses through nanoparticle-coated thin films. Interest in HHG in solids has been increased dramatically, though this process was demonstrated using the mid-infrared laser sources. The difficulties related to the absorption of generated harmonics in UV and XUV ranges during propagation through solids can be diminished while using the thin films containing nanoparticles.

The main difference of the present study compared to refs 42 and 43 is the analysis of resonance enhancement of the harmonics in the region of $\sim 47 \text{ nm}$ during the propagation of the femtosecond pulses through the tin plasma. The analysis, particularly, includes the application of the tunable source in the near-infrared range, which allowed for the tuning of the order of the harmonic being enhanced (from the 28th to the 29th order),

which allowed for the identification of the spectral range where the highest enhancement of single harmonics was achieved. The important finding in the case of the two-color pump study was the appearance of the exceptionally strong 18th harmonic of 806 nm radiation notably exceeding the earlier analyzed 17th harmonic achieved during the single-color pump of Sn laser-induced plasma. Our present study shows that the closeness of the wavelength of the harmonic with the ionic transition possessing large oscillator strength (as in the case of the almost perfect coincidence of the H17 ($\lambda = 47.4$ nm) and $4d^{10}5s^25p^2P_{3/2} \rightarrow 4d^95s^25p^2 (^1D)(^2D_{5/2})$ transition ($\lambda = 47.8$ nm)) does not necessarily lead to the stronger enhancement compared with the neighbor harmonic (H18, in our case). Notice that the latter harmonic became available due to the interaction of the weak second field (403 nm) with the strong fundamental wave (806 nm).

This contradiction was considered in our paper and different scenarios were suggested, which can, to some extent, clarify the observation of the large enhancement of the higher-order harmonic (H18) compared with the one coinciding with the strong ionic transition. The decrease of the oscillator strength of this transition, in the case of nanoparticle and molecular states of tin, as well as the influence of the collective processes when the harmonic in the region of anomalous dispersion of the ionic transition becomes quasi-phase-matched with the driving field, can be the reasons of the observed contradiction with the earlier accepted vision of the resonance-enhancement of a single harmonic in plasma. Thus, the meaning of the reexamination of the earlier reported resonance enhancement of a single harmonic is related to the approach differing from earlier suggested theories and assumptions of the necessity of perfect coincidence of the harmonic and transition wavelengths [9,10,28,33,38,42,43].

As it was underlined, the application of a near-infrared single-color pump did not result in efficient tunable odd harmonics generation to demonstrate the effect of the tunable single harmonic enhancement, due to the reasons described in our manuscript. Because of this, we used only a two-color pump (NIR and H2) to extend the harmonic emissions up to the spectral region where the enhancement of harmonics can be achieved.

The important novelty in this approach is the application of the tunable source of femtosecond pulses, allowing for the analysis of the most suitable conditions for single harmonic enhancement. The comparison of HHG in atomic and nanoparticle plasmas is another approach, allowing for the demonstration of the role of the morphology of harmonic emitters on the enhancement factor of a single harmonic.

5. Conclusions

In conclusion, we have compared the resonance-induced enhancement of single harmonic emissions during the propagation of ultrafast pulses through tin-containing laser-induced plasmas. The analysis of the dynamics of LIPs produced on a Sn bulk target and a Sn NP target has shown the range of the optimal delays between heating and driving pulses (130–180 ns), at which the maximal harmonic yield can be achieved. The similarity of this parameter for two plasmas allows us to suggest the mechanism of energy transfer during ablation, resulting in similar kinetic energy of each ingredient of ejected species.

The enhancement of the 17th and 18th harmonics of 806 nm pulses was analyzed in the case of single-color and two-color pumps of plasma, showing up to a 12-fold enhancement of even harmonics compared with the neighboring orders in the latter case. We have compared the single-atomic Sn and Sn nanoparticles-containing plasmas to demonstrate a distinction in the enhancement factor of the single harmonic in the case of tunable near-infrared pulses. We have shown the enhancement of a single harmonic in the vicinity of the $4d^{10}5s^25p^2P_{3/2} \rightarrow 4d^95s^25p^2$ transitions of Sn II ions and demonstrated how this process depends on the constituency of the plasma components at different conditions of the target ablation.

The application of tunable (1280–1440 nm) radiation from the optical parametric amplifier allowed us to demonstrate the variations of single harmonic enhancement using a tunable two-color pump of Sn-containing plasma. Our studies using tunable NIR pulses at

the fluence of an HP of $F = 1.6 \text{ J cm}^{-2}$ did not reveal that resonance-related processes lead to the enhancement of the harmonic yield, which suggests that the tuning of ionic transitions should not be the main factor leading to the cancellation of the resonance-related effect. Meanwhile, the presence of tiny NPs and clusters and single-particle species appeared in LIPs during the disintegration of large (70 nm) original aggregates of Sn atoms allows for the formation of conditions for the involvement of tin ions in the enhancement of single harmonics in the vicinity of ionic transitions possessing strong oscillator strength.

Author Contributions: Conceptualization, R.A.G., H.K.; methodology, R.A.G.; formal analysis, R.A.G., H.K.; investigation, R.A.G., H.K.; writing—original draft preparation, R.A.G.; writing—review and editing, R.A.G., H.K.; visualization, R.A.G.; supervision, H.K.; funding acquisition, R.A.G., H.K. All authors have read and agreed to the published version of the manuscript.

Funding: This research was funded by JSPS KAKENHI (grant number 24760048), ERDF (grant number 1.1.1.5/19/A/003), State Assignment to Higher Educational Institutions of Russian Federation (grant number FZGU-2020-0035), grant and the Common Research Facility at the American University of Sharjah (grant number FRG AS1801).

Institutional Review Board Statement: Not applicable.

Informed Consent Statement: Not applicable.

Data Availability Statement: The data that support the findings of this study are available from the corresponding author upon reasonable request.

Conflicts of Interest: The authors declare no conflict of interest.

References

1. Sanpera, A.; Watson, J.B.; Lewenstein, M.; Burnett, K. Harmonic-generation control. *Phys. Rev. A* **1996**, *54*, 4320–4328. [[CrossRef](#)]
2. Taïeb, R.; Vénier, V.; Wassaf, J.; Maquet, A. Roles of resonances and recollisions in strong-field atomic phenomena. II. High-order harmonic generation. *Phys. Rev. A* **2003**, *68*, 033403. [[CrossRef](#)]
3. Milošević, D.B. Theoretical analysis of high-order harmonic generation from a coherent superposition of states. *J. Opt. Soc. Am. B* **2006**, *23*, 308–315. [[CrossRef](#)]
4. Milošević, D.B. High-energy stimulated emission from plasma ablation pumped by resonant high-order harmonic generation. *J. Phys. B* **2007**, *40*, 3367–3376. [[CrossRef](#)]
5. Ivanov, I.A.; Kheifets, A.S. Resonant enhancement of generation of harmonics. *Phys. Rev. A* **2008**, *78*, 053406. [[CrossRef](#)]
6. Kulagin, I.A.; Usmanov, T. Efficient selection of single high-order harmonic caused by atomic autoionizing state influence. *Opt. Lett.* **2009**, *34*, 2616–2618. [[CrossRef](#)]
7. Chen, J.; Zeng, B.; Liu, X.; Cheng, Y.; Xu, Z. Wavelength scaling of high-order harmonic yield from an optically prepared excited state atom. *New J. Phys.* **2009**, *11*, 113021. [[CrossRef](#)]
8. Frolov, M.F.; Manakov, N.L.; Starace, A.F. Potential barrier effects in high-order harmonic generation by transition-metal ions. *Phys. Rev. A* **2010**, *82*, 023424. [[CrossRef](#)]
9. Milošević, D.B. Resonant high-order harmonic generation from plasma ablation: Laser intensity dependence of the harmonic intensity and phase. *Phys. Rev. A* **2010**, *81*, 023802. [[CrossRef](#)]
10. Strelkov, V. Role of autoionizing state in resonant high-order harmonic generation and attosecond pulse production. *Phys. Rev. Lett.* **2010**, *104*, 123901. [[CrossRef](#)]
11. Tudorovskaya, M.; Lein, M. High-order harmonic generation in the presence of a resonance. *Phys. Rev. A* **2011**, *84*, 013430. [[CrossRef](#)]
12. Ackermann, P.; Münch, H.; Halfmann, T. Resonantly-enhanced harmonic generation in argon. *Opt. Express* **2012**, *20*, 13824–13832. [[CrossRef](#)]
13. Ngoko Djiokap, J.M.; Starace, A.F. Resonant enhancement of the harmonic-generation spectrum of beryllium. *Phys. Rev. A* **2013**, *88*, 053412. [[CrossRef](#)]
14. Ganeev, R.A.; Wang, Z.; Lan, P.; Lu, P.; Suzuki, M.; Kuroda, H. Indium plasma in the single- and two-color mid-infrared fields: Enhancement of tunable harmonics. *Phys. Rev. A* **2016**, *93*, 043848. [[CrossRef](#)]
15. Wahyutama, I.S.; Sato, T.; Ishikawa, K.L. Time-dependent multiconfiguration self-consistent-field study on resonantly enhanced high-order harmonic generation from transition-metal elements. *Phys. Rev. A* **2019**, *99*, 063420. [[CrossRef](#)]
16. Cipura, F.; Halfmann, T. Resonantly enhanced harmonic generation via dressed states with large Autler–Townes splitting. *J. Opt. Soc. Am. B* **2019**, *36*, 2777–2783. [[CrossRef](#)]
17. Ngoko Djiokap, J.M.; Starace, A.F. Origin of the multiphoton-regime harmonic-generation plateau structure. *Phys. Rev. A* **2020**, *102*, 013103. [[CrossRef](#)]
18. Liang, J.; Lai, Y.H.; Fu, W.; Shan, Y.; Yu, W.; Guo, C. Observation of resonance-enhanced high-order harmonics from direct excitation of metal nanoparticles with femtosecond pulses. *Phys. Rev. A* **2020**, *102*, 053117. [[CrossRef](#)]

19. Akiyama, Y.; Midorikawa, K.; Matsunawa, Y.; Nagata, Y.; Obara, M.; Tashiro, H.; Toyoda, K. Generation of high-order harmonic using laser-produced rare-gas-like ions. *Phys. Rev. Lett.* **1992**, *69*, 2176–2779. [[CrossRef](#)]
20. Kubodera, S.; Nagata, Y.; Akiyama, Y.; Midorikawa, K.; Obara, M.; Tashiro, H.; Toyoda, K. High-order harmonic generation in laser-produced ions. *Phys. Rev. A* **1993**, *48*, 4576–4581. [[CrossRef](#)]
21. Wahlström, C.-G.; Borgström, S.; Larsson, J.; Pettersson, S.-G. High-order harmonic generation in laser-produced ions using a near-infrared laser. *Phys. Rev. A* **1995**, *51*, 585–592. [[CrossRef](#)] [[PubMed](#)]
22. Theobald, W.; Wülker, C.; Schäfer, F.R.; Chichkov, B.N. High-order harmonic generation in carbon vapor and low charged plasma. *Opt. Commun.* **1995**, *120*, 177–185. [[CrossRef](#)]
23. Ganeev, R.A.; Redkorechev, V.I.; Usmanov, T. Optical harmonics generation in low-temperature laser produced plasma. *Opt. Commun.* **1997**, *135*, 251–258. [[CrossRef](#)]
24. Krushelnick, K.; Tighe, W.; Suckewer, S. Harmonic generation from ions in underdense aluminum and lithium-fluorine plasmas. *J. Opt. Soc. Am. B* **1997**, *14*, 1687–1695. [[CrossRef](#)]
25. Ganeev, R.A.; Singhal, H.; Naik, P.A.; Chakravarty, U.; Arora, V.; Chakera, J.A.; Khan, R.A.; Raghuramaiah, M.; Kumbhare, S.R.; Kushwaha, R.P.; et al. Optimization of the high-order harmonics generated from silver plasma. *Appl. Phys. B* **2007**, *87*, 243–250. [[CrossRef](#)]
26. Singhal, H.; Arora, V.; Rao, B.S.; Naik, P.A.; Chakravarty, U.; Khan, R.A.; Gupta, P.D. Dependence of high-order harmonic intensity on the length of preformed plasma plumes. *Phys. Rev. A* **2009**, *79*, 023807. [[CrossRef](#)]
27. Pertot, Y.; Elouga Bom, L.B.; Bhardwaj, V.R.; Ozaki, T. Pencil lead plasma for generating multimicrojoule high-order harmonics with a broad spectrum. *Appl. Phys. Lett.* **2011**, *98*, 101104. [[CrossRef](#)]
28. Elouga Bom, L.B.; Haessler, S.; Gobert, O.; Perdrix, M.; Lepetit, F.; Hergott, J.-F.; Carré, B.; Ozaki, T.; Salières, P. Attosecond emission from chromium plasma. *Opt. Express* **2011**, *19*, 3677–3682. [[CrossRef](#)] [[PubMed](#)]
29. Pertot, Y.; Chen, S.; Khan, S.D.; Elouga Bom, L.B.; Ozaki, T.; Chang, Z. Generation of continuum high-order harmonics from carbon plasma using double optical gating. *J. Phys. B* **2012**, *45*, 074017. [[CrossRef](#)]
30. Kumar, M.; Singhal, H.; Chakera, J.A.; Naik, P.A.; Khan, R.A.; Gupta, P.D. Study of the spatial coherence of high order harmonic radiation generated from preformed plasma plumes. *J. Appl. Phys.* **2013**, *114*, 033112. [[CrossRef](#)]
31. Ganeev, R.A.; Suzuki, M.; Kuroda, H. Quasi-phase-matching of high-order harmonics in multiple plasma jets. *Phys. Rev. A* **2014**, *89*, 033821. [[CrossRef](#)]
32. Singhal, H.; Naik, P.A.; Kumar, M.; Chakera, J.A.; Gupta, P.D. Enhanced coherent extreme ultraviolet emission through high order harmonic generation from plasma plumes containing nanoparticles. *J. Appl. Phys.* **2014**, *115*, 033104. [[CrossRef](#)]
33. Ganeev, R.A.; Suzuki, M.; Yoneya, S.; Kuroda, H. Resonance-enhanced harmonic generation in nanoparticle-containing plasmas. *J. Phys. B* **2015**, *48*, 165401. [[CrossRef](#)]
34. Rosenthal, N.; Marcus, G. Discriminating between the role of phase matching and that of the single-atom response in resonance plasma-plume high-order harmonic generation. *Phys. Rev. Lett.* **2015**, *115*, 133901. [[CrossRef](#)]
35. Fareed, M.A.; Thiré, N.; Mondal, S.; Schmidt, B.E.; Légaré, F.; Ozaki, T. Efficient generation of sub-100 eV high-order harmonics from carbon molecules using infrared laser pulses. *Appl. Phys. Lett.* **2016**, *108*, 124104. [[CrossRef](#)]
36. Fareed, M.A.; Strelkov, V.V.; Thiré, N.; Mondal, S.; Schmidt, B.E.; Légaré, F.; Ozaki, T. High-order harmonic generation from the dressed autoionizing states. *Nature Commun.* **2017**, *8*, 16061. [[CrossRef](#)] [[PubMed](#)]
37. Wöstmann, M.; Splittthoff, L.; Zacharias, H. Control of quasi-phase-matching of high-harmonics in a spatially structured plasma. *Opt. Express* **2018**, *26*, 14524–14531. [[CrossRef](#)] [[PubMed](#)]
38. Fareed, M.A.; Strelkov, V.V.; Singh, M.; Thiré, N.; Mondal, S.; Schmidt, B.E.; Légaré, F.; Ozaki, T. Harmonic generation from neutral manganese atoms in the vicinity of the giant autoionization resonance. *Phys. Rev. Lett.* **2018**, *121*, 023201. [[CrossRef](#)]
39. Abdelrahman, Z.; Khohlova, M.A.; Walke, D.J.; Witting, T.; Zair, A.; Strelkov, V.V.; Marangos, J.P.; Tisch, J.W.G. Chirp-control of resonant high-order harmonic generation in indium ablation plumes driven by intense few-cycle laser pulses. *Opt. Express* **2018**, *26*, 15745–15755. [[CrossRef](#)]
40. Kumar, M.; Singhal, H.; Chakera, J.A. High order harmonic radiation source for multicolor extreme ultraviolet radiography of carbon plumes. *J. Appl. Phys.* **2019**, *125*, 155902. [[CrossRef](#)]
41. Singh, M.; Fareed, M.A.; Laramée, A.; Isgandarov, E.; Ozaki, T. Intense vortex high-order harmonics generated from laser-ablated plume. *Appl. Phys. Lett.* **2019**, *115*, 231105. [[CrossRef](#)]
42. Suzuki, M.; Baba, M.; Ganeev, R.; Kuroda, H.; Ozaki, T. Anomalous enhancement of single high-order harmonic using laser ablation tin plume at 47 nm. *Opt. Lett.* **2006**, *31*, 3306–3308. [[CrossRef](#)]
43. Ganeev, R.A.; Strelkov, V.V.; Hutchison, C.; Zaïr, A.; Kilbane, D.; Khokhlova, M.A.; Marangos, J.P. Experimental and theoretical studies of two-color pump resonance-induced enhancement of odd and even harmonics from a tin plasma. *Phys. Rev. A* **2012**, *85*, 023832. [[CrossRef](#)]
44. Freeman, J.R.; Harilal, S.S.; Diwakar, P.K.; Verhoff, B.; Hassanein, A. Comparison of optical emission from nanosecond and femtosecond laser produced plasma in atmosphere and vacuum conditions. *Spectrochim. Acta B* **2013**, *87*, 43. [[CrossRef](#)]
45. Duffy, G.; van Kampen, P.; Dunne, P. 4d-5p transitions in the extreme ultraviolet photoabsorption spectra of SnII and SnIII. *J. Phys. B* **2001**, *34*, 3171–3182. [[CrossRef](#)]
46. Lan, P.; Takahashi, E.; Midorikawa, K. Wavelength scaling of efficient high-order harmonic generation by two-color infrared laser fields. *Phys. Rev. A* **2010**, *81*, 061802. [[CrossRef](#)]

47. Liang, J.; Venkatesh, M.; Boltaev, G.S.; Ganeev, R.A.; Lai, Y.H.; Guo, C. Investigation of resonance-enhanced high-order harmonics by two-component laser-produced plasmas. *Atoms* **2021**, *9*, 1. [[CrossRef](#)]
48. Ganeev, R.A.; Boltaev, G.S.; Kim, V.V.; Zhang, K.; Zvyagin, A.I.; Smirnov, M.S.; Ovchinnikov, O.V.; Redkin, P.V.; Wöstmann, M.; Zacharias, H.; et al. Effective high-order harmonic generation from metal sulfide quantum dots. *Opt. Express* **2018**, *26*, 35013–35023. [[CrossRef](#)]
49. Ganeev, R.A.; Boltaev, G.S.; Kim, V.V.; Venkatesh, M.; Zvyagin, A.I.; Smirnov, M.S.; Ovchinnikov, O.V.; Wöstmann, M.; Zacharias, H.; Guo, C. High-order harmonic generation using quasi-phase matching and two-color pump of the plasmas containing molecular and alloyed metal sulfide quantum dots. *J. Appl. Phys.* **2019**, *126*, 193103. [[CrossRef](#)]